Diminished Glucose Transport and Phosphorylation in Alzheimer's Disease Determined by Dynamic FDG-PET

Morand Piert, Robert A. Koeppe, Bruno Giordani, Stanley Berent and David E. Kuhl
Division of Nuclear Medicine, Department of Internal Medicine, and Neuropsychology Program, Department of Psychiatry, University of Michigan Medical Center, Ann Arbor, Michigan

Using dynamic [^{18}F]fluorodeoxyglucose (FDG) and PET, kinetic rate constants that describe influx (K_1) and efflux (k_2) of FDG as well as phosphorylation (k_3) and dephosphorylation (k_4) were determined in patients with probable Alzheimer's disease and similarly aged normal controls. **Methods:** The regional cerebral metabolic rate for glucose (CMR_{glu}) was calculated from individually fitted rate constants in frontal, temporal, parietal and occipital cerebral cortex, caudate nucleus, putamen, thalamus and cerebellar cortex. Dynamic PET scans were obtained in normal controls (n = 10, mean age = 67) and Alzheimer's disease patients (n = 8, mean age = 67) for 60 min following injection of 10 mCi of FDG. **Results:** The Alzheimer's disease group was characterized by decreases of the CMR_{glu} ranging from 13.3% in the frontal to 40.9% in the parietal cortex, which achieved significance in all regions except the thalamus. K_1 was significantly reduced in the parietal ($p < 0.01$) and temporal cortices ($p < 0.05$). Significant declines in k_3 were found in the parietal ($p < 0.005$), temporal and occipital cortex, and in the putamen and cerebellum ($p < 0.05$). The rate constants k_2 and k_4 were unchanged in the Alzheimer's disease group. **Conclusion:** These data suggest that hypometabolism in Alzheimer's disease is related to reduced glucose phosphorylation activity as well as diminished glucose transport, particularly in the most metabolically affected areas of the brain, the parietal and temporal cortex.

Key Words: PET; Alzheimer's disease; kinetic rate constants; glucose metabolism; glucose transport; hexokinase activity

J Nucl Med 1996; 37:201–208

Fluorine-18-fluorodeoxyglucose (FDG) has been used widely with PET imaging to study glucose metabolism in Alzheimer's disease. Many investigations have verified a reduced utilization rate for glucose (CMR_{glu}) in the cerebral cortex, predominantly in the posterior temporal and parietal regions (*1–5*). Progressive dementia is accompanied by a further decrease of the CMR_{glu} in affected regions (*2,6,7*). In spite of these well-defined metabolic disturbances, questions remain about the underlying mechanisms responsible for the altered glucose utilization.

Dynamic PET offers the ability to investigate the initial metabolic steps of glucose metabolism. A three-compartmental model (*8*) allows the estimation of glucose influx (K_1) and efflux (k_2) across the blood-brain-barrier (BBB) as well as calculation of the phosphorylation rate for FDG at the hexokinase step within the tissue compartment (k_3). The hydrolysis of FDG-6-phosphate back to FDG (k_4) can be estimated by scanning for 1 hr, although with relatively high uncertainty.

Although glucose metabolism in the brain has been investigated extensively with PET, the results have been ambiguous. Similarly, our knowledge about glucose-rate constants in different brain disorders is still limited. Evidence for the alteration of rate constants in Alzheimer's disease derives from histological and biochemical findings. The characteristic amyloid deposition in and around the cerebral blood vessels in Alzheimer's disease patients (*9*), including endothelium and arterioles (*10*), accompanied with thickening of the capillary basement membrane (*11*) may lead to a diminished glucose transport (K_1) across the BBB. In biopsies of Alzheimer's disease patients, measurement of the hexose transporter protein is decreased markedly in the microvessels of the cerebral cortex compared to normal brain (*12*). Previous dynamic FDG-PET studies yielded inconclusive results in attempting to examine the initial steps of glucose metabolism by estimating individual kinetic rate constants. For example, , Friedland et al. (*13*) were unable to show significant alterations in rate constant estimates in an Alzheimer's disease brain. Later, Jagust et al. (*14*) found significant reductions of K_1 in the frontal and temporal cortex without significant changes in other rate constants.

Evidence for phosphorylation deficiencies is also limited. Sorbi et al. (*15*) found decreased hexokinase activity in skin cultured fibroblasts and leukocytes of Alzheimer's disease patients, but the relationship to cerebral hexokinase activity is uncertain. Measurement of the hexokinase activity in postmortem brain tissue showed a marked decline in Alzheimer's disease compared to age-matched controls (*16*). These data, however, require careful interpretation because enzyme activity is particularly sensitive to postmortem changes and tissue freezing (*17,18*).

We can interpret the continued coupling of cerebral blood flow (CBF) and glucose metabolism in Alzheimer's disease (*19*) as suggesting that we should expect both transport and phosphorylation to be abnormal in Alzheimer's patients. This prediction stems from the following:

1. A decrease in cerebral blood flow should cause a similar or smaller decrease in K_1, since K_1 equals flow multiplied by the single-pass extraction fraction E_0 (which may increase when flow decreases), but does not cause a decrease in the estimate of k_3.
2. A decrease in the number of glucose transporters will cause a decrease only in K_1, not in k_3.
3. A decrease in the number of neurons due to tissue atrophy should also cause a change only in the estimate of K_1, not in k_3.
4. Examination of the formula for calculating the metabolic rate of glucose (Eq. 1) reveals that a reduction of K_1 alone results in a considerably smaller reduction of CMR_{glu} (see Discussion).

Therefore, the coupling of CBF and metabolism in Alzheimer's disease is not likely to be explained by a simple decrease in K_1, which in turn does not cause metabolic rate to be reduced by the same extent. Thus, it is reasonable to expect that k_3 will be

Received Nov. 4, 1994; revision accepted Jun. 29, 1995.
For correspondence or reprints contact: R.A. Koeppe, PhD, Division of Nuclear Medicine, 3480 Kresge III, Box 0552, University of Michigan, Ann Arbor, MI 48109.

decreased in Alzheimer's disease, as could be caused by damage to the neurons, or more specifically to the synapses, instead of total loss of the neuron, which as stated above, causes a change in the estimate of K_1.

We have undertaken this study to help clarify the issues related to the mechanisms and effects of Alzheimer's disease. Dynamic FDG-PET studies provide information differentiating transport and phosphorylation processes and, in addition, are not based on the use of population average rate constants obtained from healthy young volunteers (*20*) as are the estimates of CMR_{glu} determined from static FDG methods. We therefore evaluated whether alteration of glucose transport and/or phosphorylation rate constants occur in Alzheimer's disease and whether the suspected alteration of the rate constants affects the accuracy of the static measurement of CMR_{glu} by comparing results from the kinetic approach with those from two common static analytical methods (*20,21*) using two different sets of standard rate constants.

MATERIALS AND METHODS

Dementia Patients

We studied eight right-handed patients (5 men, 3 women; aged 59–74 yr; mean age 66.8 ± 6.0 yr) with a clinical diagnosis ranging from mild to severe Alzheimer's disease. All patients fulfilled the NINCDS-ADRDA criteria for probable Alzheimer's disease (*22*). Each patient suffered from a progressive cognitive decline for at least 1 yr prior to the study and was not taking any medication considered to have influence on glucose metabolism or cerebral blood flow. Neuropsychological testing also was completed to confirm NINCDS-ADRDA criteria guidelines concerning cognitive impairment. Excluded were all cases of cerebrovascular disease, diabetes mellitus or hyperglycemia (glucose level > 125 mg/100 ml plasma during the scan), previous cranial traumata, encephalitis, drug or alcohol abuse, mental retardation, family history of neurologic or psychiatric illness or other dementing disease. General medical and neurological examinations, including several laboratory tests were performed specifically to exclude thyroid diseases, vitamin B12 or folate deficiency. None of the patients were taking any acute or chronic medications known to affect glucose metabolism at the time of the scan.

Patients' cognitive impairments were graded by several neuropsychological tests including: (a) Full Scale IQ (FSIQ; (*23*)); (b) Wechsler Memory Scale Memory Quotient (WMSMQ; (*23*)); (c) Blessed Dementia Rating (BDR; (*24*)); (d) Mini-Mental State Examination (MMS; (*25*)); and (e) Hamilton Depression Scale (HD; (*26*)). Dementia was further rated by the Washington University Clinical Dementia Rating (CDR; (*27*)).

Control Subjects

Ten right-handed normal volunteers (4 men, 6 women; aged 37–79 yr; mean age s.d. 66.9 ± 16.4 yr) were medically and neurologically screened and given laboratory tests to verify appropriate general and mental health status. None of the controls were taking any acute or chronic medications at the time of the scan. Informed consent was obtained from each subject or legal guardian. Ethical permission was obtained from the Institution Review Board of the University of Michigan, Ann Arbor, MI.

Radiotracer

Fluorine-18-FDG was prepared by direct nucleophilic exchange on a quaternary 4-aminopyridium resin (*28*). Radiochemical purity, as assessed by thin-layer chromatography, was uniformly >97%. Radioactivity at injection-time was 10 ± 1 mCi for each subject.

Scanning Procedure

Scanning was performed on a tomograph with a reconstructed resolution of approximately 7 mm FWHM within planes and 7–8 mm FWHM axially. Each subject was examined in a fasting state with eyes open, ears unplugged in a quiet and moderately lit room. Subjects were placed in a comfortable supine position and restrained across the forehead by a small band. None of the subjects were sedated for the examination. A dynamic sequence of 15 PET scans was performed on each of the subjects for 60 min following radiotracer administration according to the following protocol: 4 × 0.5 min, 3 × 1 min, 2 × 2.5 min, 2 × 5 min, 4 × 10 min. The scanned field of view covered 10 cm, starting 1.0 cm above the canthomeatal line. Arterial blood samples were drawn from the radial artery of the opposite forearm into heparinized syringes as rapidly as possible for the first 2 min following injection of FDG and then at progressively longer intervals throughout the remainder of the study. Plasma was separated and the radioactivity was counted in a NaI well counter. Arterial plasma glucose levels were determined by a standard enzymatic method averaged across three plasma samples obtained throughout the scan. Subjects with unstable glucose levels (maximum difference between samples: 25 mg/100 ml plasma) were excluded from the study.

Image Processing

Images were reconstructed by filtered backprojection using a Shepp and Logan 0.35 filter and corrected for attenuation by a standard ellipse method resulting in 128 × 128 pixel images for the entire dynamic sequence (15 frames × 15 planes). Radioactive fiducial markers were placed on the patient's scalp prior to the scan and an automated motion correction routine was used to define the bead locations on a single base frame (considered to be the standard orientation) and then reorient all other frames to the base frame (*29*). Radioactivities measured in tissue and plasma were corrected for decay and adjusted for time shift between the brain and radial artery.

Cerebral cortical regions of interest (ROIs) were drawn individually according to a standard neuroanatomical and computerized tomographic atlas (*30*) for the right and left frontal cortex, right and left temporal cortex, right and left parietal cortex and a single occipital region excluding the visual cortex. For the right and left caudate, putamen, thalamus and cerebellar cortex, standardized ROIs were placed in individually drawn ROIs by centering the standard ROI to the maximum of the individual ROI.

Mathematical Model

In both groups, kinetic parameters were estimated from the tissue and arterial plasma activity curves by a standard nonlinear least-squares analysis using the Marquardt algorithm (*31,32*). A standard three-compartmental, four-parameter tracer kinetic model configuration (*20*) extending the original work of Sokoloff et al. (*8*) was used, but with the addition of a vascular compartment. In all, five parameters were estimated from the 60-min dynamic sequence; the cerebral blood volume fraction (CBV), K_1, k_2, k_3 and k_4. Parameters K_1 and k_2 described forward and backward tracer transport across the BBB. Parameters k_3 and k_4 describe phosphorylation and dephosphorylation of FDG within the tissue compartments. Kinetic CMR_{glu} was calculated directly from the individually fitted rate constants, using the averaged plasma glucose concentration (C_P) and a LC of 0.52 (*33*) as follows:

$$CMR_{glu} = \frac{C_P}{LC} \times \frac{K_1 \times k_3}{k_2 + k_3}. \qquad \text{Eq. 1}$$

To compare different static CMR_{glu} measurement approaches with the CMR_{glu} results obtained from the individually fitted rate constants, we calculated the static CMR_{glu} from a summed image containing counts between 30 and 60 min postinjection. Static

TABLE 1
Clinical Data and Neuropsychological Test Results

Patient no.	Age at study (yr)	Sex	Age at onset (yr)	CDR	MMS	FSIQ	WMS	BDR	HD
1	60	M	55	1	9	68	56	7.5	1
2	62	M	56	1	15	74	69	10.5	8
3	68	F	65	0.5	23	93	89	5.5	5
4	66	M	53	2	13	75	65	8	5
5	59	F	54	0.5	23	90	80	5	11
6	72	M	67	1	23	101	94	0	0
7	73	M	68	1	20	82	74	6.5	3
8	74	F	69	1	19	96	79	6	3
Mean	66.8	—	60.9	1.0	18.1	84.9	75.8	6.1	4.5
s.d.	6.0	—	7.0	0.5	5.3	11.9	12.5	3.0	3.6

CDR = clinical dementia rating, MMS = mini-mental state examination; FSIQ = full scale IQ; WMS = Wechsler memory scale memory quotient; BDR = Blessed dementia rating; HD = Hamilton depression scale.

CMR_{glu} was then calculated with an LC of 0.52 with two different methods [U = UCLA method: (*20*), W = Wisconsin method: (*21*)] and two sets of standard rate constants [set 1: $K_1 = 0.084$, $k_2 = 0.193$, $k_3 = 0.096$, $k_4 = 0.007$ (from normals scanned previously at the University of Michigan); set 2: $K_1 = 0.102$, $k_2 = 0.130$, $k_3 = 0.062$, $k_4 = 0.0068$ (*20*)] resulting in 4 different static approaches (W1 = Wisconsin method and rate constant set 1; W2 = Wisconsin method and rate constant set 2; U1 = UCLA method and rate constant set 1; U2 = UCLA method and rate constant set 2). Both methods use a formula that is based on sets of standard or population average rate constants and a factor that attempts to correct for the difference between the FDG concentration predicted by the population average rate constants and that measured by the PET scanner, as given in Equation 2:

$$CMR_{glu} = \frac{C_P}{LC} \times \frac{K_{1pop} \times k_{3pop}}{k_{2pop} + k_{3pop}} CF, \qquad \text{Eq. 2}$$

where CF is the correction factor. The PET scan measures the total FDG tissue concentration (C_i) which equals the sum of the free (C_e) plus phosphorylated (C_m) FDG concentrations ($C_i = C_e + C_m$). C_e and C_m can only be calculated assuming the rate constants K_1-k_4 are known. The UCLA method assumes that the best correction factor for estimating an individual's regional metabolic rate is given by the ratio of the individual's regional tracer concentration in the phosphorylated compartment to that predicted by calculations from the population average rate constants. Since only C_i can be determined directly, C_m is be approximated by $C_i - C_e$. Thus, CF takes the form:

$$CF = \frac{(C_i)_{meas} - (C_e)_{pop}}{(C_m)_{pop}}, \qquad \text{Eq. 3}$$

where $(C_i)_{meas}$ is the measured PET value and $(C_e)_{pop}$ and $(C_m)_{pop}$ are calculated from population average rate constants (*20*).

The Wisconsin method assumes that the best correction factor for estimating an individual's regional metabolic rate is given by the ratio of the individual's measured total tracer concentration to that predicted by from calculations using the population average rate constants. With this assumption, CF becomes:

$$CF = \frac{(C_i)_{meas}}{(C_e)_{pop} + (C_m)_{pop}}, \qquad \text{Eq. 4}$$

where $(C_i)_{meas}$, $(C_e)_{pop}$ and $(C_m)_{pop}$ are the same as in Eq. 3 (*21*). Each method works better under different conditions; in general, the UCLA method more accurately corrects for changes in k_3, while the Wisconsin method better accounts for changes in K_1 and k_2 (*21*).

Statistical Analysis

The reported averages represent the arithmetic mean of both hemispheres and the s.d. across subjects. Rate constant estimates and metabolic rates in all regions were compared by means of one-way analysis of variance, including tests for homogeneity of group variances using the Bartlett test. For equal group variances ($p \geq 0.05$), data were compared by the Tukey studentized range method. For differing group variances ($p < 0.05$), Student's t-tests for differences between groups with unequal variances were performed based on the Behrens-Fisher t′ distribution. We used stepwise regression analysis to describe the accuracy of different static approaches in predicting the dynamic estimate of CMR_{glu} and also determined the correlation coefficients between the kinetic and various static methods. All statistical tests were corrected for multiple comparisons. Differences between groups were considered significant when comparisons exceeded 95% confidence limits ($p < 0.05$). All statistical tests were performed with the Systat statistical software package.

RESULTS

Patient history and representative neuropsychological test results are summarized in Table 1. Age at study, sex and plasma glucose level were not significantly different between groups. Alzheimer's disease subjects ranged from mild to severely demented as expressed by the CDR (mean 1.0 ± 0.6) and MMS (mean 17.7 ± 6.2). None of our patients reached the exclusion criteria of a Hamilton depression score of 19 or greater.

Figure 1 shows the static scan estimation of CMR_{glu} from method W1 using the 30–60-min data for typical subjects of the Alzheimer's disease and control groups. These images were used to draw the ROIs and generally contained about 3.0 million true coincidence events per direct slice.

The result of a five-parameter model fit of the PET data (K_1-k_4 and CBV) using the arterial input function is shown for four brain regions in Figure 2. Uncertainties of the parameter estimates expressed by the percent coefficient of variation (% COV = s.d./mean × 100) varied with the ROI size, varied with the individual rate parameters, as well as varying between groups. Uncertainties were generally higher in the small regions, such as basal ganglia, compared to the larger cortical regions. Parameter K_1 was the most stable rate constant in all regions for both groups with a COV ranging from 13% to 29%. Uncertainties in k_3 were higher, ranging from 26% to 56%. The rate constants k_2 and k_4 showed the highest variability with uncertainties up to 129% for k_4. The kinetic CMR_{glu} estimates

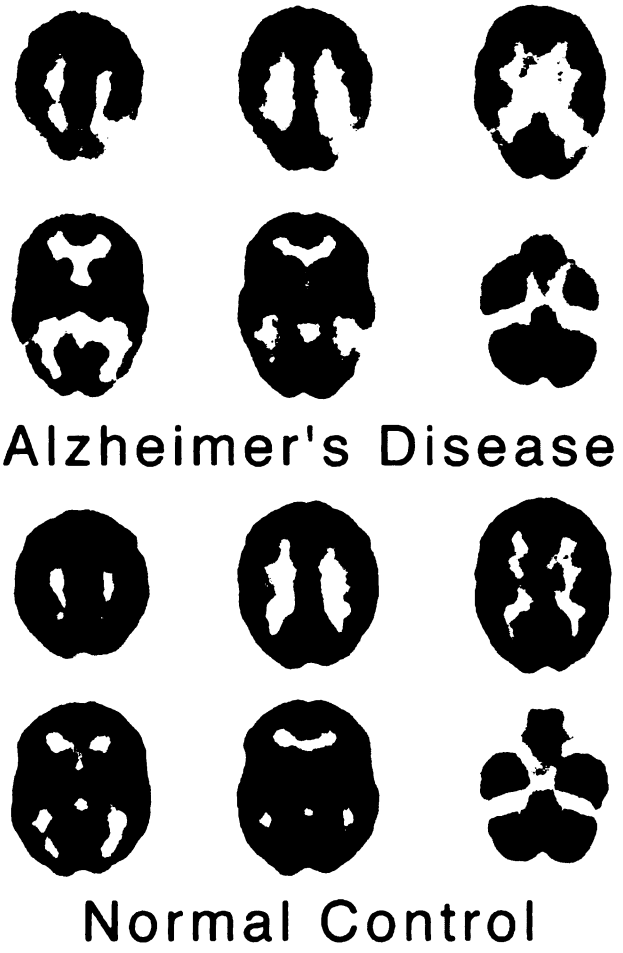

FIGURE 1. Glucose metabolic rate images in a patient and control subject. Static scan estimations of CMR_{glu} from method W1 using 30–60-min data are shown.

showed lower variabilities, comparable to K_1, with COVs ranging between 11 and 30%.

Table 2 gives the mean rate constant estimates and s.d. and the kinetic and static estimates of CMR_{glu} for eight brain regions in Alzheimer's disease patients and control. Only small differences in kinetic CMR_{glu} were observed between hemispheres. Therefore, all calculations were performed with data averaged over both hemispheres. In Alzheimer's disease patients, kinetic CMR_{glu} was decreased in all brain regions compared controls, which reached significance in all regions except the thalamus, probably due to the higher interindividual variability. Cortical reductions of the kinetic CMR_{glu} varied between 13.3% in the frontal ($p < 0.05$) and 40.9% in the parietal cortex ($p < 0.001$). Decreases in the kinetic CMR_{glu} in the putamen (−25.5%, $p < 0.001$), caudate nucleus (−20.5%, $p < 0.05$) and cerebellar cortex (−17.2%, $p < 0.05$) were significant as well. The rate constant K_1 was significantly reduced in the parietal ($p < 0.01$) and temporal cortex ($p < 0.05$). The mean value of k_3 was decreased in all regions, but due to the high uncertainties in the parameter estimates, this was significant only in the parietal cortex ($p < 0.005$), cerebellar, occipital, temporal cortex and putamen ($p < 0.05$). The estimates for rate constants k_2 and k_4 were not significantly different between the two groups in any region.

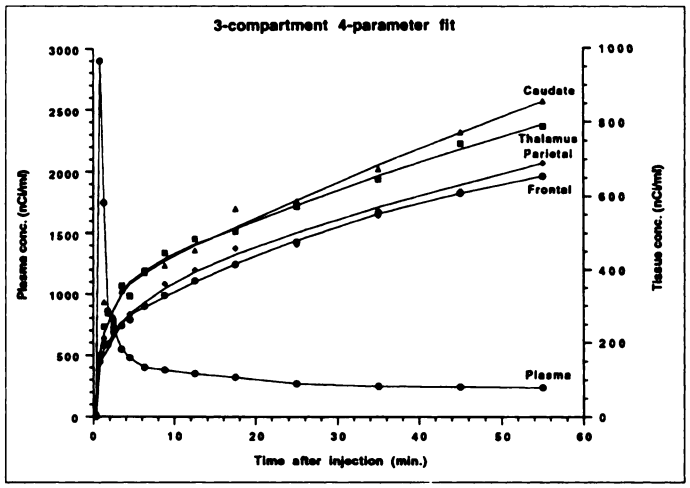

FIGURE 2. Characteristic time-courses of decay-corrected FDG concentration in plasma, frontal and parietal cortex, caudate nucleus and thalamus for a normal control subject. Solid lines represent least-squares fits to the data from a three-compartment, four-parameter model.

Kinetic measurement is considered to be more accurate than static imaging in estimating the true CMR_{glu} because individual rate constants are taken into account (*34,35*). To investigate the effects of altered glucose rate constants on the accuracy of static FDG-PET, we compared the kinetic CMR_{glu} with two static methods each with two sets of rate constants (Table 2). Generally, kinetic CMR_{glu} was correlated highly with each of the four static measures in the control subjects (correlation coefficients between 0.84 and 0.97). In Alzheimer's disease subjects, where rate constants are altered, we found lower correlation coefficients between 0.59 and 0.89. The W1 approach was the only method that was correlated significantly with the kinetic CMR_{glu} in all regions with calculated correlation coefficients ranging from 0.74 (occipital cortex) to 0.85 (caudate nucleus). Taking the kinetic estimates as the true values, static measures overestimated CMR_{glu} in most subjects. CMR_{glu} in control subjects ranked as follows: kinetic $CMR_{glu} < W2 < W1 < U2 < U1$. In the Alzheimer's disease group, in whom regional CMR_{glu} is decreased, the estimates from the U2 approach were closer to the kinetic estimates of CMR_{glu} due to the difference in correction factors (Eqs. 3, 4) used by the two single-scan methods (*21*). When transport is less than the population average value, CMR_{glu} is underestimated when using the UCLA method (*21,36,37*), which partially cancells the overestimations seen in controls and in less affected regions in Alzheimer's patients. In the cerebellar cortex, where kinetic analysis was used to determine statistically significant decreases in CMR_{glu}, none of the static approaches yielded significant differences between patients and controls. Using stepwise regression analysis, however, none of the four combinations of static method and rate constant sets was found to predict kinetic CMR_{glu} more accurately than any other combination. In regions where significant differences were detected between groups, the level of significance for the kinetic measures was consistently higher than for any of the static approaches.

DISCUSSION

Characteristic lesions for Alzheimer's disease are cortical neurofibrillary tangles, senile plaques, vascular amyloid and neuronal losses (*38,39*). Particularly, the degeneration involves basal medial temporal limbic areas, the posterior cingulate gyrus and superior parietal lobule and is somewhat less marked the inferior parietal lobule and inferior temporal gyrus (*40*). The predominant posterior-temporal and parietal cortical glucose hypometabolism matches the pathologically most affected regions. We observed a significant reduction of the kinetic CMR_{glu} in all cortical regions and the basal ganglia. The highest

TABLE 2
Kinetic Rate Constant and CMR_{glu} Estimates in Patients Compared to Controls

Region	Kinetic parameter	Normal controls (n = 10) Mean ± s.d.	Alzheimer's disease (n = 8) Mean ± s.d.	Static method	Normal controls (n = 10) Mean ± s.d.	Alzheimer's disease (n = 8) Mean ± s.d.
Parietal cortex	K_1	0.093 ± 0.021	0.067 ± 0.013***	U1	8.77 ± 1.92	6.04 ± 1.30****
	k_2	0.148 ± 0.060	0.109 ± 0.037	U2	8.28 ± 1.96	5.35 ± 1.29****
	k_3	0.179 ± 0.073	0.070 ± 0.028***	W1	8.05 ± 1.64	5.78 ± 1.20***
	k_4	0.017 ± 0.009	0.013 ± 0.008	W2	7.52 ± 1.54	5.46 ± 1.07***
	CMR_{glu}	7.54 ± 1.71	4.45 ± 1.16*****			
Temporal cortex	K_1	0.100 ± 0.018	0.082 ± 0.017*	U1	9.35 ± 2.04	7.48 ± 0.86*
	k_2	0.166 ± 0.059	0.142 ± 0.040	U2	8.87 ± 2.07	6.83 ± 0.83**
	k_3	0.183 ± 0.067	0.117 ± 0.048*	W1	8.52 ± 1.73	6.95 ± 0.83*
	k_4	0.013 ± 0.008	0.012 ± 0.007	W2	7.97 ± 1.64	6.59 ± 0.75*
	CMR_{glu}	7.99 ± 1.77	6.15 ± 0.78**			
Frontal cortex	K_1	0.099 ± 0.019	0.082 ± 0.017	U1	9.61 ± 2.34	7.48 ± 1.06
	k_2	0.141 ± 0.050	0.142 ± 0.040	U2	9.17 ± 2.38	6.82 ± 1.00**
	k_3	0.165 ± 0.061	0.117 ± 0.048	W1	8.78 ± 2.00	6.95 ± 1.00*
	k_4	0.013 ± 0.007	0.012 ± 0.007	W2	8.20 ± 1.87	6.58 ± 0.91*
	CMR_{glu}	8.10 ± 1.90	6.16 ± 0.88**			
Occipital cortex	K_1	0.090 ± 0.025	0.080 ± 0.023	U1	8.25 ± 1.91	6.67 ± 1.22*
	k_2	0.133 ± 0.048	0.151 ± 0.095	U2	7.84 ± 1.56	6.13 ± 0.86*
	k_3	0.176 ± 0.086	0.101 ± 0.049*	W1	7.69 ± 1.50	6.28 ± 1.11*
	k_4	0.013 ± 0.007	0.010 ± 0.007	W2	7.19 ± 1.40	5.95 ± 1.07
	CMR_{glu}	7.10 ± 1.53	5.38 ± 0.82**			
Thalamus	K_1	0.131 ± 0.029	0.119 ± 0.016	U1	11.48 ± 3.52	9.76 ± 1.30
	k_2	0.16 ± 0.066	0.194 ± 0.094	U2	11.15 ± 3.42	9.16 ± 1.30
	k_3	0.137 ± 0.054	0.117 ± 0.066	W1	10.40 ± 2.81	8.83 ± 1.18
	k_4	0.012 ± 0.008	0.007 ± 0.009	W2	9.75 ± 2.66	8.36 ± 1.05
	CMR_{glu}	9.27 ± 2.78	7.57 ± 1.51			
Caudate nucleus	K_1	0.119 ± 0.020	0.106 ± 0.021	U1	11.39 ± 2.18	9.52 ± 1.20*
	k_2	0.170 ± 0.090	0.176 ± 0.040	U2	10.79 ± 2.17	8.81 ± 1.21*
	k_3	0.188 ± 0.086	0.124 ± 0.041	W1	10.11 ± 1.83	8.63 ± 1.08
	k_4	0.016 ± 0.013	0.012 ± 0.012	W2	9.50 ± 1.79	8.18 ± 1.00
	CMR_{glu}	9.40 ± 2.02	7.48 ± 0.9**			
Putamen	K_1	0.132 ± 0.031	0.114 ± 0.025	U1	12.23 ± 2.72	9.75 ± 1.09*
	k_2	0.161 ± 0.075	0.181 ± 0.064	U2	11.84 ± 2.76	9.15 ± 1.10*
	k_3	0.166 ± 0.044	0.115 ± 0.046*	W1	10.95 ± 2.28	8.82 ± 0.98*
	k_4	0.010 ± 0.006	0.006 ± 0.006	W2	10.25 ± 2.17	8.35 ± 0.89*
	CMR_{glu}	10.09 ± 2.23	7.51 ± 1.19***			
Cerebellar cortex	K_1	0.134 ± 0.024	0.129 ± 0.027	U1	9.20 ± 1.78	8.45 ± 1.20
	k_2	0.190 ± 0.059	0.204 ± 0.072	U2	8.90 ± 1.91	7.82 ± 1.12
	k_3	0.122 ± 0.034	0.088 ± 0.032*	W1	8.54 ± 1.59	7.62 ± 1.37
	k_4	0.013 ± 0.007	0.009 ± 0.006	W2	7.99 ± 1.50	7.34 ± 1.04
	CMR_{glu}	7.98 ± 1.71	6.61 ± 0.72*			

*$p < 0.05$; **$p < 0.02$; ***$p < 0.01$; ****$p < 0.005$; *****$p < 0.001$
Also given are CMR_{glu} estimates from four static approaches.

reductions were observed in the parietal cortex (−40.9%, $p < 0.001$). Hypometabolism was accompanied by reductions of K_1 and k_3 in several cortical and subcortical regions. Friedland et al. (*13*) studied 16 Alzheimer's disease patients with dynamic FDG-PET compared to seven healthy controls. The scanning protocol (limited to 45 min total scan time), resolution restrictions of the tomograph and arterialized venous blood sampling may have contributed to their inability to detect significant changes in rate constant estimates, although both K_1 and k_3 were slightly decreased in the Alzheimer's disease group. Jagust et al. (*14*) found a significant decrease of K_1 in the frontal and temporal cortex of six Alzheimer's disease patients compared to seven normal controls. High uncertainties of the parameter estimates and the small subject number, however, may have accounted for the lack of significance in the observed reduction in k_3.

We have used a dynamic FDG study to demonstrate decreased forward glucose transport (K_1) and phosphorylation (k_3) in the most affected brain regions of Alzheimer's disease patients: the parietal and temporal cortices. In addition, k_3 was significantly decreased in the putamen, cerebellar and occipital cortex. High intersubject variability contributed to the lack of significance in other regions, although the regional group means of the rate constants K_1 and k_3 across subjects were generally decreased. The observed high uncertainties of parameter estimates are in the same range as reported for young (*20,36*) and elderly (*41,42*) normal volunteers and do not differ substantially from those previously reported for Alzheimer's patients (*13,14*).

Glucose enters the brain by a facilitated diffusion process through glucose transporters (*43*). Two isoforms of the glucose transporter, GLUT-1 and GLUT-3, have been identified in the

human brain. GLUT-1 is primarily responsible for the transport of glucose across the BBB, whereas GLUT-3 probably controls glucose transport into neurons (*44*). FDG-PET cannot determine whether reduced glucose transport in Alzheimer's disease is decreased at the BBB, between the BBB and neuron or at the neuronal cell membrane itself. The perivascular deposition of beta-amyloid combined with thickening of the capillary basement membrane, which are often seen in Alzheimer's disease, might suggest BBB involvement (*10,11,45*). Evidence for the alteration of the glucose transport is derived from in vitro studies of the glucose transporter protein in Alzheimer's disease. Kalaria et al. (*12*) reported a marked decrease of the hexose transporters in isolated brain microvessels and in membrane preparations of the frontal and temporal neocortex and hippocampus in Alzheimer's disease, whereas no abnormalities were noticed in the cerebellum and putamen. Harik (*46*) suggested that the density of glucose transporters in brain endothelium is downregulated probably as the result of a lowered glucose demand rather than a direct result of the hypometabolism observed in Alzheimer's disease.

Along with the reduced glucose transport (K_1) in the parietal and temporal cortex, we identified a significant decline of k_3 in Alzheimer's disease, which represents reduced phosphorylation by the hexokinase enzyme within the tissue compartment. The published results of hexokinase activity in Alzheimer's disease from in vitro studies are controversial. Meier-Ruge et al. (*47*) reported significantly lower enzyme activities for hexokinase and phosphofructokinase in Alzheimer's disease autopsy homogenates of the temporal lobe compared with age matched controls. In contrast, Liguri et al. (*48*) reported increased hexokinase activity in subcortical but not cortical structures of autopsy samples in a few Alzheimer's disease patients. Marcus et al. (*49*) combined in vitro determination of the hexokinase activity in brain microvessel preparations and in vivo dynamic [^{11}C]deoxyglucose PET to address hexokinase activity in Alzheimer's disease. They found a significant decrease in hexokinase activity in autopsied brain and a reduction of k_3 in their [^{11}C]deoxyglucose tracer study. Since the hexokinase activity is, under steady-state conditions, the rate limiting step for glucose utilization to the brain (*50–52*), this would be of considerably greater pathophysiological importance than a reduction of glucose transport rate alone.

Tissue heterogeneity is known to cause alterations to rate constants estimates. Schmidt et al. (*53*) concluded from simulation studies that dynamic FDG imaging with the four-parameter, three-compartment model artificially increases k_4, subsequently also k_3, and to a lesser extent k_2, when applied to heterogeneous tissues in image sequences of less than 120 min. As a result, the use of this kinetic modeling approach was found to overestimate CMR_{glu} in heterogeneous tissues. In fact, our estimates for k_4 and k_3 are higher than those reported for normal subjects when data were acquired over many hours (*20*) or a previous set of normal subjects in our laboratory when a fixed value of 0.007 min^{-1} was used for k_4. Thus, our high values for k_3 and k_4 likely are due to tissue heterogeneity. There is, however, no obvious reason that the effects of tissue heterogeneity were significantly greater in our control group than in our patient group, which would be necessary to yield artificially increased k_3 values only in the control group. In addition, since we did not find significant differences in k_2 or k_4 between Alzheimer's disease patients and control subjects, we consider it unlikely that effects of tissue heterogeneity are responsible for the marked decreases in k_3 observed in Alzheimer's patients.

Since we detected significant reductions in K_1 and k_3 rate constants in several brain regions in Alzheimer's patients, we evaluated the effect of diminished glucose rate constants on the accuracy of static FDG-PET measurement by comparing the kinetic CMR_{glu} with different variations of the static method as described above (W1, W2, U1, U2). This evaluation was not aimed at showing one method or set of population average rate constants to be better than another but was performed to investigate two issues: (a) whether data obtained from static methods may yield artifactual results in patients with Alzheimer's disease that have different rate constant values than normal controls and (b) whether results from static methods are similar to, but merely less powerfully statistical, than those from more complex dynamic analysis.

With the exception of the W2 approach, the other static methods overestimated CMR_{glu} relative to the kinetic approach by approximately 10%–20%. Overestimation of CMR_{glu} by static measurement was also seen by Sasaki et al. (*54*) using pixel-by-pixel analysis to determine regional rate constants in young normal volunteers. This overestimation is likely due, in part, to the use of population average rate constants that were determined many years earlier from lower resolution scanners but are now applied to scans from modern higher resolution tomographs. Sasaki et al. (*54*) reported a correlation coefficient of 0.9 for the kinetic CMR_{glu} with the U2 method in a single region. In the control group, the correlations between the kinetic and each different static approach were comparably high ($r = 0.84-0.97$ for all regions). In Alzheimer's disease subjects, however, in whom rate constants were altered, correlations between the dynamic and static methods were considerably lower. Only the W1 approach was significantly correlated with the kinetic CMR_{glu} in all regions. Because the observed values for the kinetic rate constants in the Alzheimer's disease group are closer to the population average values of rate constant set 2 (*20*) and because of the poorer performance of the Wisconsin method to errors in the assumption of the value of k_3, the U2 method may be expected to detect differences between these two groups of subjects better than the other static methods. In fact, after the kinetic approach, the U2 method did show the highest level of significance in differentiating the metabolic rates of the two groups (Table 2). Stepwise regression analysis, however, showed none of the four static approaches was more accurate than any other. These data suggest that because changes in the glucose rate constants are accounted for, kinetic measures have a higher sensitivity for discriminating altered glucose metabolism in degenerative brain diseases than do static measures, at least for the small sample sizes common in the majority of PET studies.

To help elucidate the underlying mechanisms in Alzheimer's disease, it is necessary to examine the changes that various effects of the disease would have on the estimated rate constants and to compare these expected changes with the observed measures. CBF and oxygen consumption in Alzheimer's disease is decreased from approximately 20% in mild to moderate dementia to 40% or more in severe dementia compared to age-matched control subjects (*55*). Regional CBF is decreased approximately in the same range as the CMR_{glu} (*56*) and remains coupled in Alzheimer's disease (*19*). Since K_1 is the product of regional CBF and the single-pass capillary extraction fraction, a decrease in flow will cause a decrease in K_1 but probably to a lesser degree since the extraction fraction will likely undergo a concomitant increase. The effect of diminished CBF on the rate constant k_3 is less clear and may depend on the cause of the flow deficit. As long as the reduction in CBF was due to tissue loss, a reduction in capillary density, or a simple decrease in flow through the existing capillary bed, then no specific reduction in k_3 would be expected. By using Equation

1, a simple fixed reduction in flow (i.e., equivalent reductions in both K_1 and k_2) is shown to result typically in a 50%–60% smaller reduction in CMR_{glu} if the hexokinase activity (k_3) remains unchanged. The magnitude of the reduction depends on the value of the term $k_3/[k_2 + k_3]$. When using the standard rate constants, the reduction in CMR_{glu} is 64% and 66% smaller than the reduction in flow for standard rate constant sets 1 and 2, respectively. If rate constants from the current study are used instead, the reductions in CMR_{glu} are still 43% and 58% smaller than the reduction in flow for controls and patients, respectively. Since CBF is typically decreased by 20%–40% in patients, reductions in CMR_{glu} of only approximately 10%–20% would be expected, and thus additional mechanisms besides reduction of CBF are needed to explain the observed deficits in CMR_{glu}.

The major determinant of glucose metabolism in the brain is synaptic activity (*57*). Terry et al. (*58*) reported that synapse loss is the major correlate of cognitive decline in Alzheimer's disease. Brain tissue atrophy, or more specifically neuronal cell loss and reduced synaptic activity, lead to decreased values of CMR_{glu} (*59*) and may also alter glucose rate constants. If brain atrophy is uniform, leading to tissue degeneration of all cell types (e.g., neurons and glial cells) and this lost tissue volume is filled by CSF, only decreases in K_1 would be observed, with no influence on k_2 or k_3 as long as the remaining synapses are functioning normally (*60*). This is seen by considering that CMR_{glu} is given by the product of the free tracer volume of distribution ($K_1/[k_2 + k_3]$) and the phosphorylation rate (k_3). This distribution volume or precursor pool volume is decreased by the uniform tissue loss while the rate constant k_3, reflecting the proportion of FDG in this volume that undergoes phosphorylation per unit of time, remains unchanged. If the tissue loss is not homogeneous but specific to the synapses as observed by Terry (*58*), then the effects on the rate constants are less clear. If the majority of glucose is used in the synapses, and if there is synapse loss which does not alter glucose delivery to the remaining tissue, without substantial atrophy of the neuron bodies or glial cells, then one would expect a decline in the k_3 rate constant, since the hexokinase activity per volume of tissue would be decreased. This scenario is consistent with our PET findings in Alzheimer's disease.

From Equation 1, we see that a given reduction in k_3 also will cause a smaller magnitude reduction in CMR_{glu}. Thus, if synapse loss alone is the cause of the metabolic declines seen in Alzheimer's disease, then the observed 20%–40% decreases in CMR_{glu} require decreases of 30%–60% in k_3. Deficits of this magnitude were seen only in the most affected regions, suggesting that a combination of the factors described above best explains the observed changes in CMR_{glu}. Thus, the coupling of flow and metabolism in diseased regions of the brain in Alzheimer's disease appears to require the existence of both transport and chemical deficits.

CONCLUSION

We observed significant reductions in both K_1 and k_3 in Alzheimer's patients compared to similar aged normal controls. We suggest that the observed reductions in glucose transport and phosphorylation in Alzheimer's disease are not just regional deficits found only in the most affected areas of the brain, i.e., parietal and temporal cortex, but are part of a general decline observed, to different degrees, in all cortical and subcortical regions throughout the entire brain. The decline in regions that appear to be affected only later in the disease may be masked by high interindividual variabilities and the small number of subjects investigated. Therefore, the described alterations in glucose utilization pathway may be a more general metabolic disturbance in degenerative brain disorders which are not necessarily accompanied by major pathological findings and merely are observed earliest in the most affected brain regions. It remains unclear, whether the observed declines in glucose transport and phosphorylation are primary deficiencies in altered glucose metabolism or are more likely the expression of functional downregulation in a neuronal network where energy demands are globally and regionally reduced. In either case, not a single, but a combination of several patho-mechanisms that contribute to the diminished rate of glucose utilization, including reduced CBF, deficiency of the glucose transporter, brain atrophy characterized by neuronal cell loss and reduced synaptic activity, are required to fully explain the hemodynamic and metabolic deficits observed in Alzheimer's disease.

ACKNOWLEDGMENTS

We thank the members of the PET/Cyclotron Facility, the Nuclear Pharmacy and the PET Imaging Suite for their excellent and extensive support. We also thank Nancy Lowenbergh for subject recruitment and Kathleen B. Welch and John Warner of the Center for Statistical Consultation and Research of the University of Michigan for their assistance. Supported in part by National Institutes of Health grants R01-NS-24896 and P01-NS-15655 awarded by NINDS, Michigan Alzheimer's Disease Research Center P50-AG-08671 and by Department of Energy grant DE-F602-87ER60561. Presented in part at the European Association of Nuclear Medicine Congress 1993 in Lausanne, Switzerland.

REFERENCES

1. Benson DF, Kuhl DE, Hawkins RA, Phelps ME, Cummings JL, Tsai SY. The fluorodeoxyglucose ^{18}F scan in Alzheimer's disease and multi-infarct dementia. *Arch Neurol* 1983;40:711–713.
2. Duara R, Grady C, Haxby J, et al. Positron emission tomography in Alzheimer's disease. *Neurology* 1986;36:879–887.
3. Foster NL, Chase TN, Mansi L, et al. Cortical abnormalities in Alzheimer's disease. *Ann Neurol* 1984;16:649–654.
4. Friedland RP, Budinger TF, Ganz E, et al. Regional cerebral metabolic alterations in dementia of the Alzheimer type: positron emission tomography with [^{18}F]fluorodeoxyglucose. *J Comp Assist Tomogr* 1983;7:590–598.
5. Peppard RF, Martin WR, Clark CM, McGeer PL, Calne DB. Cortical glucose metabolism in Parkinson's and Alzheimer's disease. *J Neuroscience Res* 1990;27:561–568.
6. Chase TN, Foster NL, Fedio P, Brooks R, Mansi L, Di Chiro G. Regional cortical dysfunction in Alzheimer's disease as determined by positron emission tomography. *Ann Neurol* 1984(suppl);S170–S174.
7. Haxby JV, Grady CL, Duara R, Schlageter N, Berg G, Rapoport SI. Neocortical metabolic abnormalities precede nonmemory cognitive defects in early Alzheimer's-type dementia. *Arch Neurol* 1986;43:882–885.
8. Sokoloff L, Reivich M, Kennedy C, et al. The [^{14}C]deoxyglucose method for the measurement of local cerebral glucose utilization: theory, procedure and normal values in the conscious and anesthetized albino rat. *J Neurochem* 1977;28:897–916.
9. Martins RN, Robinson PJ, Chleboun KO, Beyreuther K, Masters CL. The molecular pathology of Amyloid deposition in Alzheimer's disease. *Molecular Neurobiology* 1991;5:389–398.
10. Glenner GG, Wong CW. Alzheimer's disease: initial report of the purification and characterization of a novel cerebrovascular amyloid protein. *Biochem Biophys Res Commun* 1984;120:885–890.
11. Mancardi GL, Perdelli F, Rivano C, Leonardi A, Bugiani O. Thickening of the basement membrane of cortical capillaries in Alzheimer's disease. *Acta Neuropathol* 1980;49:79–84.
12. Kalaria RN, Harik SI. Reduced glucose transporter at the blood-brain barrier and in cerebral cortex in Alzheimer's disease. *J Neurochem* 1989;53:1083–1088.
13. Friedland RP, Jagust WJ, Huesman RH, et al. Regional cerebral glucose transport and utilization in Alzheimer's disease. *Neurology* 1989;39:1427–1434.
14. Jagust WJ, Seab JP, Huesman RH, et al. Diminished glucose transport in Alzheimer's disease: dynamic PET studies *J Cereb Blood Flow Metab* 1991;11:323–330.
15. Sorbi S, Mortilla M, Piacentini S, Tonini S, Amaducci L. Altered hexokinase activity in skin cultured fibroblasts and leukocytes from Alzheimer's disease patients. *Neuroscience Letters* 1990;117:165–168.
16. Iwangoff P, Armbruster R, Enz A, Meier-Ruge W. Glycolytic enzymes from human autopsy brain cortex: normal aged and demented cases. *Mech Aging Dev* 1980;14:203–209.
17. Bird ED, Gale JS, Spokes EGS. Huntington's chorea: post mortem activity of enzymes involved in cerebral glucose metabolism. *J Neurochem* 1977;29:539–545.
18. Iwangoff P, Reichlmeier K, Enz A, Meier-Ruge W. Neurochemical findings in physiological aging of the brain. *Interdisc Topics Gerontol* 1979;15:13–33.

19. Hara M, Minoshima S, Foster NL, Kuhl DE. Is regional cerebral blood flow coupled with glucose metabolism in Alzheimer's disease [Abstract]? *J Nucl Med* 1993; 34(suppl):116P.
20. Phelps ME, Huang SC, Hoffman EJ, Selin C, Sokoloff L, Kuhl DE. Tomographic measurements of local cerebral glucose metabolic rate in humans with [^{18}F]2-fluoro-2-deoxy-D-glucose: validation of the method. *Ann Neurol* 1979;6:371–388.
21. Hutchins GD, Holden JE, Koeppe RA, et al. Alternative approach to single-scan estimation of cerebral glucose metabolic rate using glucose analogs, with particular application to ischemia. *J Cereb Blood Flow Metab* 1984;4:35–40.
22. McKhann G, Drachman D, Folstein M, Katzman R, Price D, Stadlan EM. Clinical diagnosis of Alzheimer's disease: report of the NINCDS-ADRDA Work Group under the auspices of Department of Health and Human Services Task Force on Alzheimer's disease. *Neurology* 1984;34:939–944.
23. Wechsler D. *The wechsler adult intelligence scale—revised manual.* New York: The Psychological Corporation; 1981.
24. Blessed G, Tomlinson BE, Roth M. The association between quantitative measures of dementia and of senile change in the cerebral grey matter of elderly subjects. *Br J Psychiatry* 1968;114:797–811.
25. Folstein MF, Folstein SE, McHugh PR. "Mini-Mental State": a practical method for grading the cognitive state of patients for the clinician. *J Psychiatr Res* 1975;12:189–198.
26. Hamilton M. Development of a rating scale for primary depression illness. *Br J Social Clinical Psychology* 1967;6:278–296.
27. Berg L. Clinical dementia rating (CDR). *Psychopharmacol Bull* 1988;25:637–639.
28. Toorongian SA, Mulholland GK, Jewett DM, Bachelor MA, Kilbourn MR. Routine production of 2-deoxy-2-[^{18}F]fluoro-D-glucose by direct nucleophilic exchange on a quaternary 4-Aminopyridinium resin. *Int J Rad Appl Instrum B* 1990;17:273–279.
29. Koeppe RA, Holthoff VA, Frey KA, Kilbourn MR, Kuhl DE. Compartment analysis of [^{11}C]flumazenil kinetics for the estimation of ligand transport rate and receptor distribution using positron emission tomography. *J Cereb Blood Flow Metab* 1991; 11:735–744.
30. Talairach J, Tournoux P. *Coplanar stereotaxic atlas of the human brain.* New York: Thieme; 1988.
31. Bevington PR. *Data reduction and error analysis for the physical sciences.* New York: McGraw-Hill; 1969;232–241.
32. Marquardt DW. An algorithm for least-squares estimation of nonlinear parameters. *J Soc Appl Math* 1963;11:431–441.
33. Reivich M, Alavi A, Wolf A, et al. Glucose metabolic rate kinetic model parameter determination in humans: the lumped constants and rate constants for [^{18}F]fluorodeoxyglucose and [^{11}C]deoxyglucose. *J Cereb Blood Flow Metab* 1985;5:179–92.
34. Heiss W-D, Pawlik G, Herholz K, Wagner R, Göldner H, Wienhard K. Regional kinetic constants and cerebral metabolic rate for glucose in normal human volunteers determined by dynamic positron emission tomography of [^{18}F]-2-fluoro-2-deoxy-D-glucose. *J Cereb Blood Flow Metab* 1984;4:212–223.
35. Lammertsma AA, Brooks DJ, Frackowiak RS, et al. Measurement of glucose utilization with [^{18}F]2-fluoro-2-deoxy-D-glucose: a comparison of different analytical methods. *J Cereb Blood Flow Metab* 1987;7:161–172.
36. Huang S-C, Phelps ME, Hoffman EJ, Sideris K, Selin CJ, Kuhl DE. Noninvasive determination of local cerebral metabolic rate of glucose in man. *Am J Physiol* 1980;238:E69–E82.
37. Huang S-C, Phelps ME, Hoffman EJ, Kuhl DE. Error sensitivity of fluorodeoxyglucose method for measurement of cerebral metabolic rate of glucose. *J Cereb Blood Flow Metab* 1981;1:391–401.
38. Katzman R. Alzheimer's disease. *N Engl J Med* 1986;313:964–973.
39. Kawai M, Kalaria RN, Harik SI, Perry G. The relationship of amyloid plaques to cerebral capillaries in Alzheimer's disease. *Am J Pathol* 1990;137:1435–1446.
40. Englund AB, Englund E. Regional pattern of degeneration in Alzheimer's disease: neuronal loss and histopathological grading. *Histopathology* 1981;5:549–564.
41. Evans AC, Diksic M, Yamamoto YL, et al. Effect of vascular activity in the determination of rate constants for the uptake of ^{18}F-labeled 2-fluoro-2-deoxy-D-glucose: error analysis and normal values in older subjects. *J Cereb Blood Flow Metab* 1986;6:724–738.
42. Hawkins RA, Phelps ME, Huang S-C, Kuhl DE. Effect of ischemia on quantification of local cerebral glucose metabolic rate in man. *J Cereb Blood Flow Metab* 1981;1:37–51.
43. Pelligrino DA, LaManna JC, Duckrow RB, Bryan RM, Harik SI Jr. Hyperglycemia and blood-brain barrier glucose transport. *J Cereb Blood Flow Metab* 1992;12:887–899.
44. Pessin JE, Bell GI. Mammalian facilitative glucose transporter family: structure and molecular regulation. *Annu Rev Physiol* 1992;54;911–930.
45. Abbott NJ, Revest PA, Romero IA. Astrocyte-endothelial interaction: physiology and pathology. *Neuropathology and Applied Neurobiology* 1992;18:424–433.
46. Harik SI. Changes in the glucose transporter of brain capillaries. *Can J Physiol Pharmacol* 1992;70:S113–S117.
47. Meier-Ruge W, Iwangoff P, Reichlmeier K. Neurochemical enzyme changes in Alzheimer's and Pick's disease. *Arch Gerontol Geriatr* 1984;3:161–165.
48. Liguri G, Taddei N, Nassi P, Latorraca S, Nediani C, Sorbi S. Changes in Na^+, K^+-ATPase, Ca^{2+}-ATPase and some soluble enzymes related to energy metabolism in brains of patients with Alzheimer's disease. *Neuroscience Letters* 1990;112:338–342.
49. Marcus DL, de Leon MJ, Goldman J, et al. Altered glucose metabolism in microvessels from patients with Alzheimer's disease. *Ann Neurol* 1989;26:91–94.
50. Furler SM, Jenkins AB, Storlien LH, Kraegen EW, Barnett D. In vivo location of the rate-limiting step of hexose uptake in muscle and brain tissue of rats. *Am J Physiol* 1991;261:E337–E347.
51. Lund-Anderson H. Transport of glucose from blood to brain. *Physiol Rev* 1979;59: 305–352.
52. Robinson PJ, Rapoport SI. Glucose transport and metabolism in the brain. *Am J Physiol* 1986;250:R127–R136.
53. Schmidt K, Mies G, Sokoloff L. Model of kinetic behavior of deoxyglucose in heterogeneous tissues in brain: a reinterpretation of the significance of parameters fitted homogeneous tissue models. *J Cereb Blood Flow Metab* 1991;11:10–24.
54. Sasaki H, Kanno I, Murakami M, Shishido F, Uemura K. Tomographic mapping of kinetic rate constants in the fluorodeoxyglucose model using dynamic positron emission tomography. *J Cereb Blood Flow Metab* 1986;6:447–454.
55. Frackowiak RS, Pozzilli C, Legg NJ, et al. Regional cerebral oxygen supply and utilization in dementia: a clinical and physiological study with ^{15}O and positron tomography. *Brain* 1981;104:753–778.
56. Prohovnik I, Mayeux R, Sackeim HA, Smith G, Stern Y, Alderson PO. Cerebral perfusion as a diagnostic marker of early Alzheimer's disease. *Neurology* 1988;38: 931–937.
57. Mata M, Fink DJ, Gainer H. Activity-dependent energy metabolism in rat posterior pituitary primarily reflects sodium pump activity. *J Neurochem* 1980;34:213–215.
58. Terry RD, Masliah E, Salmon DP, et al. Physical basis of cognitive alterations in Alzheimer's disease: synapse loss is the major correlate of cognitive impairment. *Ann Neurol* 1991;30:572–580.
59. Herscovitch P, Auchus AP, Gado M, Chi D, Raichle ME. Correction of positron emission tomography data for cerebral atrophy. *J Cereb Blood Flow Metab* 1986;6: 120–124.
60. Koeppe R, Foster N, Kuhl DE. Tissue atrophy alone cannot explain parietal hypometabolism in PET studies of Alzheimer's disease [Abstract]. *J Nucl Med* 1989;3(suppl):895.